Ocean acidification alters morphology of all otolith types in Clark's anemonefish (*Amphiprion clarkii*)

Robert Holmberg [Corresp., 1], **Eric Wilcox-Freeburg** [1], **Andrew L Rhyne** [2], **Michael F Tlusty** [1], **Alan Stebbins** [1], **Steven W Nye Jr.** [1], **Aaron Honig** [1], **Amy E Johnston** [1], **Christine M San Antonio** [1], **Bradford Bourque** [2], **Robyn E Hannigan** [1]

[1] School for the Environment, University of Massachusetts at Boston, Boston, Massachusetts, United States

[2] Department of Biology, Marine Biology and Environmental Science, Roger Williams University, Bristol, Rhode Island, United States

Corresponding Author: Robert Holmberg
Email address: Robert.Holmberg001@umb.edu

Ocean acidification, the ongoing decline of surface ocean pH and [CO_3^{2-}] due to absorption of surplus atmospheric CO_2, has far-reaching consequences for marine biota, especially calcifiers. Among these are teleost fishes, which internally calcify otoliths, critical elements of the inner ear and vestibular system. There is evidence in the literature that ocean acidification increases otolith size and alters shape, perhaps impacting otic mechanics and thus sensory perception. However, existing analyses of otolith morphological responses to ocean acidification are limited to 2-dimensional morphometrics and shape analysis. Here, we reared larval Clark's anemonefish, *Amphiprion clarkii* (Bennett, 1830), in various seawater pH treatments analogous to future ocean scenarios in a 3x-replicated experimental design. Upon settlement, we removed all otoliths from each individual fish and analyzed them for treatment effects on morphometrics including area, perimeter, and circularity; further, we used scanning electron microscopy to screen otoliths visually for evidence of treatment effects on lateral development, surface roughness, and vaterite replacement. Our results corroborate those of other experiments with other taxa that observed otolith growth with elevated pCO_2, and provide evidence that lateral development and surface roughness increased as well; we observed at least one of these effects in all otolith types. Finally, we review previous work investigating ocean acidification impacts on otolith morphology and hypotheses concerning function, placing our observations in context. These impacts may have consequences teleost fitness in the near-future ocean.

AUTHOR COVER PAGE

TITLE

Ocean acidification alters morphology of all otolith types in Clark's anemonefish (*Amphiprion clarkii*)

AUTHOR NAMES

Robert J Holmberg[a], Eric Wilcox-Freeburg[a], Andrew L Rhyne[b], Michael F Tlusty[a], Alan Stebbins[a], Steven W Nye Jr.[a], Aaron Honig[a], Amy E Johnston[a], Christine M San Antonio[a], Bradford Bourque[b], Robyn E Hannigan[a]

AUTHOR AFFILIATIONS

[a]School for the Environment, University of Massachusetts Boston, MA, 100 William T Morrissey Blvd, Boston, MA 02125

[b]Department of Biology, Marine Biology and Environmental Science, Roger Williams University, 1 Old Ferry Rd, Bristol, RI 02809

CORRESPONDING AUTHOR

Robert J Holmberg

Robert.Holmberg001@umb.edu

ABSTRACT

Ocean acidification, the ongoing decline of surface ocean pH and [CO_3^{2-}] due to absorption of surplus atmospheric CO_2, has far-reaching consequences for marine biota, especially calcifiers. Among these are teleost fishes, which internally calcify otoliths, critical elements of the inner ear and vestibular system. There is evidence in the literature that ocean acidification increases otolith size and alters shape, perhaps impacting otic mechanics and thus sensory perception. However, existing analyses of otolith morphological responses to ocean acidification are limited to 2-dimensional morphometrics and shape analysis. Here, we reared larval Clark's anemonefish, *Amphiprion clarkii* (Bennett, 1830), in various seawater pH treatments analogous to future ocean scenarios in a 3x-replicated experimental design. Upon settlement, we removed all otoliths from each individual fish and analyzed them for treatment effects on morphometrics including area, perimeter, and circularity; further, we used scanning electron microscopy to screen otoliths visually for evidence of treatment effects on lateral development, surface roughness, and vaterite replacement. Our results corroborate those of other experiments with other taxa that observed otolith growth with elevated pCO_2, and provide evidence that lateral development and surface roughness increased as well; we observed at least one of these effects in all otolith types. Finally, we review previous work investigating ocean acidification impacts on otolith morphology and hypotheses concerning function, placing our observations in context. These impacts may have consequences teleost fitness in the near-future ocean.

INTRODUCTION

Since the advent of the industrial revolution, humankind has inadvertently relocated a significant volume of carbon to the troposphere, where it now resides as a greenhouse gas, warming the earth via radiative forcing (IPCC, 2013). Global warming, however, is not the sole consequence of surplus atmospheric CO_2: the surface ocean has absorbed approximately 30% of anthropogenic CO_2 emissions (Mikaloff Fletcher et al., 2006; Le Quéré et al., 2010), contributing to ocean acidification (Caldeira and Wickett, 2003). While this absorption is an important sink, serving to abate the greenhouse effect (IPCC, 2013), it has consequences for marine ecosystems. Following diffusion, aqueous CO_2 impacts seawater chemistry in two ways: it causes decreases

in pH and the concentration of carbonate (CO_3^{2-}) (Doney et al., 2009). Both are expected to impact the fitness of marine biota, with cascading effects up to the ecosystem level (Fabry et al., 2008). From population abundances to community shifts, ocean acidification has the potential to alter the ecological landscape of the ocean (Gaylord et al., 2015).

The declining availability of free CO_3^{2-} is particularly worrisome due to its implications for marine calcifiers, which use calcium carbonate ($CaCO_3$) to form body structures including shells, teeth, and spines. Surface waters are normally supersaturated with CO_3^{2-}, but as [CO_3^{2-}] decreases, calcifiers may struggle to precipitate $CaCO_3$ (Gattuso and Buddemeier, 2000). Furthermore, if seawater is undersaturated with respect to calcium carbonate minerals (e.g. aragonite, Ω_{Ar}), existing structures may readily dissolve (Orr et al., 2005). A vast body of literature expounds ocean acidification's anticipated effects on calcifier fitness in the future ocean, demonstrating variable degrees of severity (Hendriks et al., 2010; Kroeker et al., 2013). Differential responses may depend on the specific biochemical pathways involved in calcification (Ries et al., 2009), biological mechanisms for buffering pH changes in body fluids (Munday et al., 2011a), energetics limiting physiological acclimation (Seibel et al., 2012), or various ecological forces acting on an organism (Kroeker et al., 2012).

Our primary interests are the diverse impacts of ocean acidification on physiology and calcification in teleost fishes. Teleostei is an extremely diverse infraclass of Actinopterygii representing the modern bony fishes, comprised of more than 30,000 species and dominating most aquatic habitats (Froese and Pauly, 2018). Heuer and Grosell (2014) reviewed numerous effects of acidification on marine teleosts, including respiratory acidosis leading to sustained elevation of blood plasma HCO_3^- (Esbaugh et al., 2012), cognitive disruption and behavioral changes linked to inhibited $GABA_A$ neurotransmitter receptor function (Nilsson et al., 2012), mixed impacts on standard and maximum metabolic rates with implications for aerobic scope (Munday et al., 2009), and more. In addition, teleosts are internal calcifiers, precipitating $CaCO_3$ in the intestinal lumen that aids water absorption and osmoregulation (Grosell, 2011), and precipitating otoliths in the inner ear that are critical for mechanoreception (Moyle and Cech, 2004); these structures may be points of vulnerability for teleosts in the near-future ocean (Ishimatsu et al., 2008; Munday et al., 2008; Heuer and Grosell, 2014).

Otoliths, or ear stones, are critical features located within the inner ear of teleost fishes, formed by precipitation of $CaCO_3$ around a protein-rich matrix and bathed in endolymph

(Panella, 1971). $CaCO_3$ supersaturation is maintained in the endolymph by proton pumps in the epithelial cells adjacent to the site of crystallization, which maintain the pH gradient required for CO_3^{2-} - HCO_3^- balance (Ishimatsu et al., 2008). Otoliths exist in three pairs, with one from each pair contained within each otolithic end organ (saccule, utricle, lagena) in each side of the head proximally ventral to the brain: the aragonitic sagittae and lapilli, traditionally believed to function for hearing and gravisense respectively, and the oft-vateritic asterisci, traditionally believed to function for hearing like the sagittae – however, these functions are not strictly delineated and may indeed overlap (Popper and Fay, 1993). When an otolith is disturbed by fish movement or sound waves, it triggers sensory hair cells (maculae) lining the interior wall of its chamber, which convert the force into electrical impulses interpreted by the brain. Likewise, otoliths function as sensory organs for detecting balance, acceleration, and sound (Fekete, 2003; Moyle and Cech, 2004).

Researchers recognize the potential for ocean acidification to impact otolith growth in teleosts, especially during the sensitive larval phase, and many have demonstrated effects experimentally (Table 1). Contrary to the hypothesis that ocean acidification will inhibit otolith growth due to dwindling CO_3^{2-} availability (Ishimatsu et al., 2008), elevated seawater pCO_2 stimulates growth of sagittae and/or lapilli in many taxa. This growth is attributed to elevated blood plasma [HCO_3^-], retained to buffer acidosis and transported into the endolymph where it becomes substrate for CO_3^{2-} aggregation (Checkley et al., 2009; Munday et al., 2011b; Heuer and Grosell, 2014). Only one study (Mu et al. 2015) observed decreased otolith size in response to elevated pCO_2. Other studies (Franke and Clemmesen, 2011; Munday et al., 2011a; Simpson et al., 2011; Frommel et al., 2013; Perry et al, 2015; Cattano et al., 2017; Martino et al., 2017; Jarrold and Munday, 2018) observed no effects of pCO_2 on otolith morphology.

The variability in otolith responses to ocean acidification is perhaps unsurprising given the diversity of life histories exhibited by teleosts and apparent critical period of development. However, evidence that acidification alters otolith size and shape has inspired hypotheses that this could interfere with otic mechanics, and thus impair sensory perception in teleosts (Munday et al., 2011b; Bignami et al., 2013b, 2014; Pimentel et al., 2014; Schade et al., 2014; Mu et al., 2015; Réveillac et al., 2015; Shen et al., 2016; Faria et al., 2017; Martino et al., 2017; Martins, 2017; Mirasole et al., 2017; Coll-Lladó et al., 2018; Jarrold and Munday, 2018). Indeed, there is some evidence that asymmetry of otolith size, shape, and mass may impair auditory/vestibular

function in some species with consequences for habitat detection and overall fitness (Lychakov and Rebane, 2005; Gagliano et al., 2008; Anken et al., 2017). Munday et al. (2011b) hypothesized that enhanced otolith growth in larval *Amphiprion percula* under ocean acidification could impact fish performance and fitness, but acknowledged that some degree of variation is normal. Others have echoed this hypothesis, adding that increased otolith size could enhance auditory sensitivity to the benefit or detriment of the fish depending on life history (Bignami et al., 2013b, 2014; Réveillac et al., 2015).

While most available studies quantified simple morphometrics to analyze pCO_2 effects on otolith morphology, the most informative among them augmented morphometrics with other analyses, including complex shape analyses (e.g. Fourier analysis) (Munday et al., 2011a,b; Simpson et al., 2011; Martino et al., 2017; Mirasole et al., 2017); mass, volume and density analyses (Bignami et al. 2013a,b); and compositional analyses (e.g. LA-ICPMS) (Munday et al., 2011b; Hurst et al., 2012; Martino et al., 2017; Mirasole et al., 2017; Coll-Lladó et al., 2018). Similarly, scanning electron microscopy can be used to screen for treatment effects on aspects of otolith morphology and composition that, although typically overlooked in simple morphometric analysis, may impact ear function. To that end, we investigated a suite of mineralogical metrics including: lateral development, defined as the degree of convexity of an otolith's lateral face; percent visible crystals, defined as an estimate of surface crystal density or grain, approximating surface roughness; crystal habit, here defined as any deviation in crystal shape from the predominant orthorhombic aragonite in sagittae and lapilli, or hexagonal vaterite in asterisci; and overall mineralogy, here defined as relative proportion of orthorhombic aragonite versus hexagonal vaterite visible on an otolith's surface. The former two metrics estimate an otolith's surface topography and texture, and the latter two metrics estimate crystal features indicative of composition, density, and stability under environmental stress. These metrics are intended as first-pass screening tools; should they yield compelling evidence of treatment differences, they could be followed with more rigorous methods to best quantify the variable (e.g., measuring otolith height directly or determining $CaCO_3$ polymorph composition with Raman spectroscopy).

Here, we investigate ocean acidification impacts on otolith morphology in larval Clark's anemonefish, *Amphiprion clarkii* (Bennett, 1830). *A. clarkii* is a teleost reef fish belonging to Pomacentridae and inhabiting shallow reefs throughout the Indo-Pacific (Froese and Pauly, 2018). We chose this species both as a novel taxon and to enable intragenus comparison with

previous work (Munday et al., 2011b). We reared *A. clarkii* in various pH treatments analogous to present and future ocean scenarios over a period of 10 days, from hatch to settlement. Our experiment included a total of 480 larvae distributed among 12 aquaria in a fully randomized and 3x-replicated design. Following the experimental trial, we removed all six otoliths (sagittae, lapilli, and asterisci) from each individual fish, performed automated morphometric analyses, and performed visual estimation and analyses according to our suite of mineralogical metrics. We also performed analyses of fish mortality, settlement timing, and somatic growth. Any differences in otolith morphology may have implications for teleost sensory perception and fitness in the near-future ocean.

MATERIALS & METHODS

Livestock: We completed all husbandry at Roger Williams University in Bristol, Rhode Island, USA (IACUC #R-11-09-13), rearing several *Amphiprion clarkii* (Bennett, 1830) broodstock pairs. Broodstock periodically laid clutches of eggs on porcelain tiles in aquaria (every 10-12 days), and we inspected them daily for quality and development. We selected the largest, healthiest clutch, removed it the night before anticipated day of hatch (around day eight post-deposition), and placed it in a separate, 50 gal hatching aquarium. We gently aerated eggs to ensure sufficient oxygen diffusion without excess agitation. Upon hatch, we randomly distributed *A. clarkii* larvae into 10 gal experimental aquaria at a density of 40 individuals per aquarium, all the while maintaining minimal agitation. Throughout the experimental trial, we fed larvae ad libitum with wild copepods from monoculture (*Pseudodiaptomus spp.*) in a background of algae (*Isochrysis spp.*). We dosed *Pseudodiaptomus spp.* to densities of 5 mL^{-1} and 1 mL^{-1} (nauplii and adults respectively), as measured using a counting wheel, and *Isochrysis spp.* twice daily to maintain a concentration of 40,000 cells mL^{-1}, as measured using a cell counter (Beckman Coulter Inc., Brea, CA).

Experimental Trial: Our experimental design consisted of four pCO_2/pH treatments selected to model various present and anticipated future ocean conditions: 1. 350 µatm/pH 8.16 (control), modern ocean conditions; 2. 800 µatm/pH 7.80, approximate conditions projected for 2100 under Representative Concentration Pathway (RCP) 8.5 (IPCC, 2013); 3. 1600 µatm/pH 7.60, nearly

double 2100 levels under RCP 8.5 (IPCC, 2013); 4. 3000 µatm/pH 7.30, a reasonable extreme given additive coastal eutrophication-induced acidification (Wallace et al., 2014). We replicated treatments three times and assigned them to 12 experimental units (aquaria) in a randomized design. We drew seawater from Mt. Hope Bay, sterilized it using sodium hypochlorite and UV light, filtered it to 1 µm, and used it to fill experimental aquaria. We completed 25% water changes every other day using drip buckets at 100 mL min^{-1}. We measured seawater salinity and temperature twice daily in all aquaria using a handheld meter (YSI, Yellow Springs, OH). We measured seawater total alkalinity once every other day in all aquaria using a tabletop autotitrator (Hanna Instruments, Smithfield, RI). We conducted the experimental trial within an environmental chamber to maintain ambient air conditions at 28°C, and covered aquaria with loose fitting lids to minimize CO_2 outgassing and evaporative heat loss. We aerated seawater with house-supplied air connected to airstones to maintain dissolved oxygen. We achieved and maintained experimental treatments by dosing CO_2 gas through the airstones using a CO_2 dosing apparatus (Wilcox-Freeburg et al., 2013) controlled by hobbyist aquarium controllers (Digital Aquatics, Woodinville, WA). We measured pH_T of each aquarium continuously using research-grade glass combination electrodes calibrated to synthetic seawater buffers (Byrne, 1987; Millero et al., 1993), prepared from analytical reagent grade chemicals (Fisher Scientific, Hampton, NH). The aquarium controller output pH_T data every 1-3 seconds via RSS feed, which we parsed/logged to a PC with a custom Python script (Wilcox-Freeburg, 2014) (Python Version 3.7.0a2; https://www.python.org/). We calculated average DIC, pCO_2, and Ω_{Ar} for each aquarium from measured seawater parameters with CO2calc (https://soundwaves.usgs.gov/2011/03/research4.html). We concluded the experimental trial after 10 days, or approximately the duration of the species' larval phase.

Data Collection: Upon conclusion of the experimental trial, and following euthanization of fish with a lethal dose of tricaine mesylate (MS-222) in seawater, we counted each individual, placed them on a Sedgewick rafter (1 mm), and photographed them with a digital camera-equipped stereomicroscope at 10x-90x magnification. We calculated mortality counts (by aquarium) by subtracting final fish counts from initial stocking density. We measured standard lengths of each individual to 1/100 mm from stereomicrographs with ImageJ (Version 1.51n; https://imagej.nih.gov/ij/), and averaged them by aquarium (arithmetic mean). Due to the natural

variation in time required for individuals to settle, some were unsettled when we ended the trial. We determined settlement visually from stereomicrographs of each fish according to overall development (i.e. presence of stripes, fin development, pigmentation, etc.), and tallied proportions of settled fish versus total remaining fish for each aquarium. We excluded unsettled fish data (standard length, otolith morphometric variables, otolith mineralogical variables) from all further analyses (sample exclusion criteria were pre-established). Next, we dissected fish using clean microsurgical techniques. We removed all six otoliths (two each of sagittae, lapilli, and asterisci) under a polarizing stereo dissection microscope. We digitally photographed each set of otoliths with the stereomicroscope at 90x magnification and subsequently mounted them to aluminum scanning electron microscopy (SEM) stubs for later analysis. We quantified area, perimeter, major axis, and minor axis of all six otoliths from all fish from stereomicrographs with custom MATLAB image analysis software (Wilcox-Freeburg, 2014) (MATLAB Version R2017b; https://www.mathworks.com/products/matlab.html). All otolith morphometrics were measured to 1/100 unit. We calculated circularity from major and minor axes $\left(\frac{\pi \times (\text{minor axis}/2)^2}{\pi \times (\text{major axis}/2)^2}\right)$. We determined aquarium means for each morphometric variable by calculating the arithmetic mean of data from all individual fish within each aquarium (grouped by otolith type and side). Due to moderate-strong correlations between standard length and otolith area and perimeter at the evaluation unit (individual fish) level (area: $r > 0.49$, perimeter: $r > 0.30$ for all otolith types/sides), we normalized otolith area and perimeter to standard length of individuals prior to calculating aquarium means. This facilitated investigation of treatment effects while accounting for potentially confounding differences in standard length between fish. Next, we imaged each individual otolith with SEM in secondary electron mode using working distance of 10 mm, spot size of 30, accelerating voltage of 10 kV, and magnification up to 3,000x. We scored otolith scanning electron micrographs visually for various mineralogy-related variables multiple times using Qualtrics survey software (Version N/A; https://www.qualtrics.com/). Six trained, independent readers scored variables including lateral development (scale of 1-5), crystal habit (orthorhombic, hexagonal, acicular, acrystalline, amorphous), percent visible crystals (5-50%), and mineralogy (proportion aragonite/vaterite on an otolith's surface interpretable by crystal habit) according to a rubric (see "Supplemental Rubric S3.pdf" for the rubric used to train and

guide readers through scoring[1]). The rubric contains reference illustrations (and in the case of the lateral development variable, micrographs) for each metric and lists categories to choose from for scoring; for each metric, the readers were asked to choose the option that best categorizes each otolith. Poor-quality micrographs due to mounting errors or broken otoliths were marked as unusable and not scored. We generated otolith-specific raw data grouped by type and side for each variable from the survey questions. We assigned each individual otolith the mode of survey scores for each variable. If a two-way mode tie occurred, we selected the lower of the modes. If a three-way mode tie occurred, we selected the median mode. For the lateral development and percent visible crystals variables, we determined aquarium means by calculating the arithmetic mean of the survey response mode for each otolith type and side, thus generating approximately continuous aquarium means from ordinal data (Norman, 2010). The mineralogy and crystal habit variables are nominal, so we determined the aquarium means by calculating the mode of the otolith modes.

Statistical Analyses: We carried out all statistical analyses using R (Version 3.4.3; https://www.r-project.org/). We considered polynomial models for all regression analyses, and performed model selection using goodness of fit tests (i.e., F-tests for general linear models and chi-squared tests for generalized linear models). We tested all binomial logistic regression models for overdispersion. All statistical tests were two-tailed. We analyzed treatment effect on fish mortality with binomial logistic regression analysis (link function = logit), with the proportion of mortality counts (per aquarium)/aquarium stocking density as the response variable and pCO_2 as the explanatory variable. We investigated treatment effect on somatic growth with regression analysis, with mean fish standard length (mm) as the response variable and pCO_2 as the explanatory variable. We investigated treatment effect on settlement time with binomial logistic regression analysis, with the proportion of settled (per aquarium)/remaining fish (per aquarium) at the end of the experimental trial as the response variable and pCO_2 as the explanatory variable. The crystal habit and mineralogy response variables exhibited no variance across any treatment and otolith type, so we excluded them from further analysis. We performed principal component analysis (PCA) on aquarium means for each otolith type and side. We ran PCA on the correlation

[1] "Core development" in the rubric has been renamed "lateral development" in the manuscript. In the rubric, "core" refers not to the otolith's core but to the center of its lateral face.

matrix between the morphometric (area, perimeter, circularity) and survey (lateral development, percent visible crystals) response variables using varimax rotation. We retained components with eigenvalues greater than or equal to 1.0. We investigated treatment effects of pCO_2 on otolith morphometrics with regression analysis, with component scores as the response variables and pCO_2 as the explanatory variable. We performed regression analysis on all components representing all otolith types and sides, and retained models in which pCO_2 significantly predicted the component.

RESULTS

Seawater Carbonate Chemistry:

Seawater carbonate chemistry parameters, including total pH (pH_T), salinity (S), temperature (T), total alkalinity (A_T), dissolved inorganic carbon (DIC), partial pressure of CO_2 (pCO_2), and the saturation state of aragonite (Ω_{Ar}) are reported as treatment means and standard deviations (for measured parameters) in Table 2.

Mortality, Settlement and Somatic Growth:

Fish mortality and settlement percentages, as well as fish standard length measurements, are reported as treatment means and standard deviations in Table 3. Despite high mortality throughout the experimental trial (Fig. 1A), we observed no difference in the odds of fish mortality between levels of treatment. However, we observed a difference in the timing of settlement between levels of treatment: in a binomial logistic regression (Fig. 1B), pCO_2 predicted the proportion of settled fish / remaining fish ($\chi^2(1, 10) = 20.55$, $p = 0.0279$). The odds of settlement decreased by an estimated 4% with each 100 µatm increase in pCO_2 (95% CI: 0% – 7%, $\text{logit}(\pi) = (-3.81E\text{-}4)x + 2.31$ where y is binomial (m,π)). pCO_2 explained approximately 38% of the variation in the odds of settlement (Nagelkerke's $R^2 = 0.38$). We also observed a difference in the somatic growth of fish between levels of treatment: in a linear regression (Fig. 1C), pCO_2 predicted fish standard length (linear regression: $F(1, 10) = 17.77$, $p = 0.0018$). Fish standard length decreased by 0.01 mm with each 100 µatm increase in pCO_2 (95% CI: 0.00 -

0.02 mm decrease, y = (-1.31E-4)x + 6.85), and pCO_2 explained approximately 60% of the variation in fish standard length ($R^2 = 0.60$).

Otolith Morphometrics and Scoring:

Unstandardized otolith area and perimeter measurements, as well as circularity measurements and estimates of two mineralogical metrics (lateral development and percent visible crystals), are reported as treatment means and standard deviations for each otolith type in Table 4. For the lateral development metric, the standard deviation of scores among the six micrograph readers was ≤ 2.23; for 73% of samples, the standard deviation was ≤ 1 (the difference between each successive category in the lateral development metric). For the percent visible crystals metric, the standard deviation of scores among the six micrograph readers was ≤ 0.21; for 22% of samples, the standard deviation was ≤ 0.05 (the minimum difference between two successive categories in the percent visible crystals metric), and for 93% of samples, the standard deviation was ≤ 0.15 (the maximum difference between two successive categories). Scoring for the crystal habit and mineralogy metrics never deviated from the norm for any otolith type in any treatment (i.e., sagittae and lapilli were consistently scored as predominantly aragonitic, exhibiting orthorhombic crystal habit; asterisci were assumed to be vateritic despite exhibiting little to no identifiable crystal habit).

Principal Component Analysis:

For each otolith type and side, PCA produced two components with eigenvalues greater than 1.0. These components, along with variances explained and loadings corresponding to each otolith metric, are reported in Table 5.

Left Sagittae (LS): RC1 correlated most strongly with lateral development, percent visible crystals, and area/SL; RC1 correlated to a lesser degree with perimeter/SL. RC2 correlated most strongly with circularity, perimeter/SL, and area/SL. Area/SL correlated more strongly with RC1 than RC2, whereas perimeter/SL correlated more strongly with RC2 than RC1. In a linear

regression (Fig. 2A), pCO_2 predicted RC1 score ($F(1, 10) = 11.98$, $p = 0.0061$). RC1 score increased by 0.07 with every 100 µatm increase in pCO_2 (95% CI: 0.03 - 0.12, $y = (7.28E\text{-}4)x - 0.98$). pCO_2 accounted for 50% of the variability in RC1 score ($R^2 = 0.50$). In summary: as pCO_2 increased, left sagittae were rendered overall larger and wider in circumference, with more pronounced lateral faces and rougher surface textures owed to greater visible crystal density.

Right Sagittae (RS): RC1 correlated most strongly with percent visible crystals, lateral development, area/SL, and perimeter/SL. RC2 correlated most strongly with circularity, perimeter/SL, and area/SL. Area/SL and perimeter/SL correlated more strongly with RC1 than RC2. In a quadratic regression (Fig. 2B), pCO_2 predicted RC1 score ($F(2, 9) = 20.56$, $p = 0.0004$, $y = (2.51E\text{-}3)x - (5.08E\text{-}7)x^2 - 1.98$). pCO_2 accounted for 78% of the variability in RC1 score ($R^2 = 0.78$). In summary: as pCO_2 increased, right sagittae responded according to the same metrics, albeit with slightly stronger responses of area/SL and perimeter/SL.

While left and right sagittae were mostly consistent in their responses between sides, the regression of left sagittae RC1 score against pCO_2 was best represented as a linear model, whereas the regression of right sagittae RC1 score against pCO_2 was best represented as a curvilinear (quadratic) model. This suggests that right sagittae RC1 score increased with pCO_2 before leveling out between the pH 7.60 and pH 7.30 treatments and decreasing, perhaps indicating asymmetry of response thresholds between sides.

Left lapilli (LL): RC1 correlated most strongly with percent visible crystals, lateral development, and circularity. RC2 correlated most strongly with area/SL and perimeter/SL ($r = 0.88$). In a quadratic regression (Fig. 2C), pCO_2 predicted RC2 score ($F(2, 9) = 10.47$, $p = 0.0045$, $y = (3.48E\text{-}3)x - (8.86E\text{-}7)x^2 - 2.25$). pCO_2 accounted for 63% of the variability in RC2 score ($R^2 = 0.63$). In summary: as pCO_2 increased, left lapilli were rendered larger and wider in circumference.

Right Lapilli (RL): RC1 correlated most strongly with perimeter/SL, area/SL, and circularity. RC2 correlated most strongly with percent visible crystals and lateral development. In a linear regression (Fig. 2D), pCO_2 predicted RC2 score ($F(1, 10) = 8.21$, $p = 0.0168$). RC2 score increased by 0.07 with every 100 µatm increase in pCO_2 (95% CI: 0.01 – 0.12, $y = (6.62E\text{-}4)x - 0.89$). pCO_2 accounted for 40% of the variability in RC2 score ($R^2 = 0.40$). In summary: as

358 pCO_2 increased, right lapilli were rendered rougher with more pronounced lateral faces despite
359 remaining approximately the same size.

360 Unlike the sagittae, the lapilli responded to treatment according to different metrics
361 depending on side. Like the sagittae, however, the lapilli exhibited differences in patterns of
362 response depending on side. As with the right sagittae, the regression of left lapilli RC2 score
363 against pCO_2 was best represented as a curvilinear (quadratic) model: area/SL and perimeter/SL
364 increased through the pH 7.60 treatment only before falling slightly in the pH 7.30 treatment. In
365 contrast, the right lapilli response was best represented as a linear model, with no sign of leveling
366 out. This may indicate asymmetry of response thresholds between sides.

367 *Left Asterisci (LA)*: RC1 correlated most strongly with perimeter/SL, area/SL, lateral
368 development, and percent visible crystals. RC2 correlated most strongly with circularity, percent
369 visible crystals, and perimeter/SL. Perimeter/SL correlated more strongly with RC1 than RC2,
370 whereas percent visible crystals correlated more strongly with RC2 than RC1. In a linear
371 regression (Fig. 2E), pCO_2 predicted RC2 score ($F(1, 9) = 5.61$, $p = 0.0420$). RC2 score
372 increased by 0.07 with every 100 µatm increase in pCO_2 (95% CI: 0.00 – 0.13, $y = (6.64E\text{-}4)x - 0.80$). pCO_2 accounted for 32% of the variability in RC2 score ($R^2 = 0.32$). In summary: as pCO_2
374 increased, left asterisci were rendered increasingly elliptical (rather than circular), rougher, and
375 wider in circumference. Notably, this is the only instance of 2-dimensional otolith shape change
376 that we observed in response to treatment, as well as the only otolith metric that decreased rather
377 than increased with increasing pCO_2.

378 *Right Asterisci (RA)*: RC1 correlated most strongly with perimeter/standard length,
379 area/SL, circularity, and percent visible crystals. RC2 correlated most strongly with lateral
380 development and percent visible crystals. Percent visible crystals correlated more strongly with
381 RC2 than RC1, but the difference was small. However, neither component predicted pCO_2 (Fig.
382 2F). In summary: right asterisci were not observed to respond to increasing pCO_2.

383 As with the lapilli, the asterisci responded differently depending on side. Indeed, the right
384 asterisci were the only otolith type/side that exhibited no response to treatment.

385

386

DISCUSSION

Fish Condition:

As might be expected when rearing many hundreds of fish in the most delicate early stages of development, *Amphiprion clarkii* larvae experienced substantial mortality throughout the experimental trial, and especially in the first few days after stocking. Specifically, 164 of the 480 stocked individuals survived until the end of the trial. Higher-than-usual mortality might be attributed in part to the stress of moving larvae immediately post-hatch. Although there is evidence in the literature of acute CO_2 toxicity in larval teleosts, this is typically observed at pCO_2 levels far exceeding those evaluated here (i.e. > 48,000 uatm) (Kikkawa et al., 2003; Ishimatsu et al., 2004; Kikkawa et al., 2004); indeed, we observed no evidence that treatment instigated fish mortality. We concede that time-series analysis of fish mortality would have been most appropriate, but due to the miniscule size and transparency of larvae throughout most of the trial, as well as low visibility in the algae-darkened aquaria, counting mortalities as they occurred was impractical. The sum of daily mortality counts did not match the difference of remaining fish from initial stocking density, so we considered time-series analysis of mortality inappropriate and used the latter for final mortality counts.

Although we observed no evidence of pCO_2 impacting mortality in *A. clarkii*, we investigated whether treatment could delay settlement and/or retard somatic growth sub-lethally. Odds of on-time settlement were inversely correlated with pCO_2 intensity, and the trend was dramatic: the 4% decrease in odds of settlement with every 100 µatm increase in pCO_2 equates to a 19% decrease with every 500 µatm increase, or roughly 20% decrease with each treatment level. We hypothesize that settlement delays could impact the later growth of *A. clarkii* as in another reef fish, *Thalassoma bifasciatum* (Victor, 1986), although this knowledge gap requires further investigation. Since settlement was evaluated just once at the end of the experimental trial, and since unsettled fish were euthanized before achieving settlement, the magnitude of settlement delay is unknown. We observed a similar sub-lethal effect of pCO_2 on somatic growth, albeit not as dramatic: though statistically significant, the reduction in fish standard lengths with increasing pCO_2 amounts to a small fraction of fish standard lengths. In summary:

treatment delayed fish settlement, but did not appreciably inhibit fish somatic growth, nor impact fish mortality.

Otolith Morphology:

Otoliths exhibited diverse responses to treatment according to type and side. In response to increasing seawater pCO_2, all three otolith types exhibited increasing perimeter and percent visible crystals, sagittae and lapilli exhibited increasing area and lateral development, and asterisci exhibited differences in shape. However, while the sagittae changed according to the same metrics regardless of side, the lapilli and asterisci changed according to different metrics depending on side. These differences reveal important things about the nature of the metrics under investigation. For example, while both sagittae responded to treatment by growing larger with more pronounced lateral faces, these effects were segregated according to side in the lapilli; this suggests that otolith area and lateral development are uncoupled rather than being two immutably conjoined metrics of growth. For reasons like this, when investigating impacts of ocean acidification or other stresses on otolith development, it is often informative to investigate each otolith independently rather than investigating one type or pooling by type without regard to side. Among the 24 studies reviewed here that analyzed ocean acidification impacts on otolith morphology, five investigated lapilli (Bignami et al., 2013a,b, 2014; Maneja et al., 2013; Shen et al., 2016; Cattano et al. 2017; Coll-Lladó et al., 2018), none investigated asterisci, and eight segregated otoliths by side during morphometric analysis (at least six of which pooled them after observing no evidence of asymmetry) (Franke and Clemmesen, 2011; Munday et al., 2011a,b; Maneja et al., 2013; Bignami et al., 2014; Mu et al., 2015; Perry et al., 2015; Réveillac et al., 2015; Martins, 2017; Jarrold and Munday 2018).

Researchers previously examined otolith development in teleost larvae reared under acidified conditions, and despite differences in methodology and model species, it is possible to draw comparisons to our own work. Notably, Munday et al.'s (2011b) study species (*Amphiprion percula*) enables intragenus comparison with *A. clarkii*. Our results are consistent with those of Munday et al. (2011b) and several others (Checkley et al., 2009; Bignami et al., 2013a,b, 2014; Maneja et al., 2013; Pimentel et al., 2014; Réveillac et al., 2015; Schade et al., 2014; Shen et al., 2016; Faria et al. 2017; Coll-Lladó et al. 2018) in that we also observed larger sagittal area at

elevated seawater pCO_2. However, Munday et al. (2011b) observed growth in left sagittae only, whereas we observed growth in both sagittae. Our results are further consistent with six of those studies (Bignami et al., 2013a,b, 2014; Maneja et al., 2013, Shen et al., 2016; Coll-Lladó et al. 2018) in that we not only observed larger sagittae but also larger lapilli at elevated pCO_2 (although we observed greater area in left lapilli only). Regarding otolith shape: our results are consistent with five studies (Maneja et al., 2013; Réveillac et al., 2015; Martins, 2017; Mirasole et al., 2017, Coll-Lladó et al., 2018) in that we observed altered otolith shape at elevated pCO_2, albeit in left asterisci only (rather than sagittae and/or lapilli).

Some of the observed effects of seawater pCO_2 on otolith development may be consequences of acid-base regulation triggered by respiratory acidosis. Heuer and Grosell (2014) reviewed the physiological impacts of elevated pCO_2 on fishes, including those related to acid-base balance and otolith calcification. Fishes are exceptional acid-base regulators, capable of normalizing pH in hours to days following onset of exposure to CO_2 concentrations more than tripling the most extreme treatment investigated here (10,000+ μatm). This is achieved primarily by metabolic adjustment: blood plasma HCO_3^- is absorbed/retained and H^+ excreted by modulating rates of transport across the gill epithelium. However, extracellular pCO_2 and HCO_3^- remain elevated following pH adjustment, and excess HCO_3^- is imported to the endolymph where it becomes substrate for CO_3^{2-} aggregation. Hydration of excess CO_2 within the saccular endolymph may further increase endolymph [HCO_3^-]. This may explain enhanced otolith size / growth rate in response to elevated seawater pCO_2 observed previously (Checkley et al., 2009; Munday et al., 2011b; Bignami et al., 2013a,b, 2014; Maneja et al., 2013; Pimentel et al., 2014; Schade et al., 2014; Réveillac et al., 2015; Shen et al., 2016; Faria et al., 2017; Mirasole et al., 2017; Coll-Lladó et al., 2018): blood plasma HCO_3^- retained to buffer respiratory acidosis moves into the endolymph, increasing endolymph [HCO_3^-] and CO_3^{2-} incorporation into the otoliths, thus enhancing net otolith calcification (Checkley et al., 2009; Munday et al., 2011b; Heuer and Grosell, 2014). This may explain the increasing area, perimeter, and lateral development that we observed in *A. clarkii*.

Otolith Function: Hypotheses and Speculation:

Since otoliths are critical components of the ears and vestibular organs (Fekete, 2003; Moyle and Cech, 2004), and since otolith asymmetry impairs hearing and kinesthesia in some fishes (Lychakov and Rebane, 2005; Gagliano et al., 2008; Anken et al., 2017), researchers have expressed concern that ocean acidification-driven changes to otolith development may challenge sensory perception in teleosts (Munday et al., 2011b; Bignami et al., 2013b, 2014; Pimentel et al., 2014; Schade et al., 2014; Mu et al., 2015; Réveillac et al., 2015; Shen et al., 2016; Faria et al., 2017; Martino et al., 2017; Martins, 2017; Mirasole et al., 2017; Coll-Lladó et al., 2018; Jarrold and Munday, 2018). Available evidence supporting these hypotheses is limited to theoretical models and rare experimental evidence outside the context of ocean acidification, but pending more conclusive analyses, this evidence warrants review. Although speculative, altered auditory/vestibular sensitivity could influence the ability of a fish to identify desirable habitat, detect prey and predators, perceive changes to water flow, and maintain kinesthetic awareness, all of which are important to larvae survival (Oxman et al., 2007; Bignami et al., 2013b). Fish that are differentially sensitive to sound and/or kinesthesia due to ocean acidification-altered otoliths could experience selective mortality from associated vectors, similar to how differential behavior due to ocean acidification is associated with selective mortality from predation in juvenile reef fish (Munday et al., 2012).

Hearing: Bignami et al. (2013b) observed increased sagittae and lapilli mass, volume, and density in larval *Rachycentron canadum* at elevated seawater pCO_2, and created a mathematical model demonstrating increased displacement amplitude of sagittae, altering maculae deformation thresholds and enabling detection of otherwise undetectable sounds. Contrary to the hypothesis that larger sagittae would enhance hearing, however, larger sagittae were associated with hearing impairment in juvenile red drum (*Sciaenops ocellatus*); those with abnormally large sagittae failed to respond to acoustic stimuli at all (Browning et al., 2012). This is probably because *Sciaenops ocellatus* sagittal mass remained constant despite greater volume (Browning et al., 2012), whereas *R. canadum* otolith mass increased with volume (Bignami et al., 2013b): entering Browning et al.'s mass and volume data into Bignami et al.'s equation for calculating otolith displacement magnitude yields a 50% lesser displacement for abnormally large *Sciaenops ocellatus* sagittae relative to normal sagittae – perhaps enough to reduce hearing sensitivity below behavioral response thresholds. This hypothesis is supported by the observation that Chinook salmon (*Oncorhynchus tshawytscha*) with at least one larger, less dense, vateritic

sagitta exhibited dramatically reduced hearing sensitivity relative to those with aragonitic sagittae of equal mass (Oxman et al., 2007), and the calculation that Atlantic salmon (*Salmo salar*) with vateritic sagittae lose otolith oscillation amplitude progressively according to degree of vaterite replacement (Reimer et al., 2016). In summary, factors influencing an otolith's density, including $CaCO_3$ polymorph and proportion of $CaCO_3$/protein, are probably better predictors of auditory/vestibular sensitivity than otolith size alone. While neither this study nor one other (Munday et al., 2011b) observed evidence of vaterite replacement in otoliths at elevated seawater pCO_2, a recent study (Coll-Lladó et al., 2018) observed calcite replacement in larval gilthead sea bream (*Sparus aurata*) sagittae and lapilli at elevated pCO_2. Like vaterite, calcite is a $CaCO_3$ polymorph less dense than aragonite (Filho et al., 2014), so ocean acidification-induced calcite replacement could similarly impair hearing in teleosts.

Kinesthesia: Besides auditory sensitivity, ocean acidification impacts on otolith morphology or composition have the potential to interfere with vestibular sensitivity: increasing otolith mass as evidenced by increasing area, perimeter, and lateral development could alter displacement amplitude and impact gravisense. It is reasonable to suggest that altered gravisense could challenge any teleost behavior involving movement, including hunting, predator avoidance, and lateralization in the water column; indeed, it could manifest as listless or kinetotic behavior akin to that observed in fishes reared under reduced gravity (Anken et al., 1998; Anken and Rahmann, 1999; Beier, 1999; Hilbig et al., 2002; Anken et al., 2017). However, evidence for these hypotheses is even more limited and speculative than that related to auditory sensitivity. Notably, larval Mozambique tilapia (*Oreochromis mossambicus*) with area-asymmetric lapilli were more susceptible to kinetoses under high quality microgravity than those with symmetric lapilli (Anken et al., 2017). Bignami et al. (2013a, 2014) observed increased sagittae and lapilli area and wider initial growth increments in larval *R. canadum* at elevated pCO_2, as well as overall larger sagittae and lapilli in larval *Coryphaena hippurus*, but did not observe compelling effects on swimming activity or critical swimming speed – metrics related to vestibular function – in either. Shen et al. (2016) observed increased sagittae and lapilli area under elevated pCO_2, but did not observe effects on gain or phase shift related to the vestibulo-ocular reflex. However, neither Shen et al. nor Bignami et al. investigated otolith asymmetry. Since pCO_2 influenced *A. clarkii* lapilli and asterisci according to different metrics depending on side, we speculate effects on gravisense in *A. clarkii* and other species exhibiting otolith asymmetry, as in Anken et al.

(2017), from ocean acidification. More research concurrently investigating fish kinesthesia and ocean acidification impacts on otolith condition and asymmetry is needed to explore this hypothesis.

Behavior: There is some empirical evidence linking anomalous otolith morphology to anomalous fish behavior, presumably following from sensory interference. Juvenile *Sciaenops ocellatus* that were hearing-impaired due to abnormally large sagittae exhibited greater visual acuity than those with normal sagittae, as measured by response to visual stimuli; Browning et al. (2012) attributed this to sensory compensation. Further, these specimens exhibited higher cortisol levels, indicating greater stress; this was attributed to a heightened startle response upon capture due to hearing impairment. Finally, the same specimens exhibited less schooling behavior, although it is unclear if this is attributable to sagittal size. Among the available studies that investigated ocean acidification impacts on otolith condition, few concurrently investigated real-world fish behavior or response to sensory cues, and those that did were unable to link them; studies either observed impacts on otolith condition without observing impacts on behavior (Bignami et al., 2013a,2014), observed impacts on behavior (i.e., impaired avoidance of reef noise) without observing impacts on otolith condition (Simpson et al., 2011), or observed impacts on neither behavior (i.e., predator recognition) nor otolith condition (Cattano et al., 2017). Given that impacts on otolith condition and fish behavior have been observed in several species, but never simultaneously, research that observes both and tests for correlation between them is needed to investigate hypotheses that the former influences the latter. Nevertheless, we hypothesize that the observed effects of pCO_2 on otolith development in *A. clarkii* could impact sensory perception and behavior in ways similar to those described above. Behavioral anomalies linked to ocean acidification effects on neurotransmitter function in teleosts (Nilsson et al., 2012; Hamilton et al., 2013; Chivers et al., 2014; Heuer and Grosell, 2014; Lai et al., 2015) do not preclude this hypothetical challenge to teleost fitness; it is a different cause-effect pathway altogether, and may intensify or moderate these anomalies.

Lateral Development and Surface Roughness:

In addition to corroborating reports of otolith growth along the x and y axes (i.e., increasing area and perimeter) in young teleosts in response to increasing seawater pCO_2, we

observed evidence for pCO_2-induced otolith growth along the z-axis (i.e., upward growth from the lateral face) in *A. clarkii*. Lateral development appears most conspicuous in sagittae, and linked to treatment in sagittae and right lapilli, although we observed it in asterisci as well. While lateral development occurs on the lateral face, which does not directly interact with maculae, it is possible this $CaCO_3$ aggregation will increase otolith mass at a magnitude greater than that which is evident from increased 2-dimensional area and perimeter. Thus, sagittae exhibiting advanced lateral development may have a wider displacement amplitude independent of area and perimeter, enhancing auditory sensitivity as in Bignami et al. (2013b). Indeed, the proportionately larger increase in sagittal and lapillar volume vs. area observed by Bignami et al. (2013b) at elevated seawater pCO_2 (as evidenced by increased area and volume but decreased surface-area-to-volume ratio) could conceivably be attributed to lateral development, if not regular growth. This hypothesis is independent of otolith composition, for which we observed no evidence of having changed, but which undermined auditory sensitivity in some studies (Oxman et al., 2007; Browning et al., 2012; Reimer et al., 2016). Also, since lateral development appears to occur on only one face of the otolith (though the medial face was not investigated here, all otoliths were imaged convex-side up, which was invariably the lateral face), its center of mass likely changes as well, with unknown consequences for otic mechanics. Changing otolith shape as evidenced by decreasing circularity in left asterisci could similarly affect maculae deformation thresholds, further impacting auditory sensitivity (Oxman et al., 2007).

Some of our otoliths appear visibly smooth on the surface, while others appear rougher due to the exposure of aragonite table edges and similar crystal activity. Estimating percent visible crystals is akin to estimating otolith surface roughness. Our observation that percent visible crystals increased with increasing pCO_2 in sagittae, right lapilli, and left asterisci is consistent with the characterization of rough-type otoliths as abnormal in other species (Béarez et al., 2005; Ma et al., 2008; Browning et al., 2012). Increasing roughness could be a symptom of haphazard $CaCO_3$ aggregation, evidence of modified protein matrix deposition, or a snapshot of an evolving $CaCO_3$ crystal habit/polymorph baseline. While roughness seems unlikely to affect otolith displacement amplitude, it could conceivably affect otic mechanics on its own. In several species of catfishes including the upside-down catfish (*Synodontis nigriventris*), it was observed that otoliths are rough on the ventral end only, driving maculae deformation by hooking them to the otolith surface (Ohnishi et al., 2002). Should it occur on the macula-oriented medial face as

with the lateral face, ocean acidification-induced otolith roughness could improve maculae grip, altering auditory and vestibular sensitivity. Furthermore, maculae could conceivably adhere to regions of the otolith surface that are normally smooth, deforming them in unusual ways and impacting sensory perception. However, these hypotheses are very speculative - more research concurrently investigating fish behavior, ocean acidification-induced otolith roughness, and maculae displacement is needed to explore this hypothesis.

CONCLUSIONS

Our work corroborates evidence of otolith growth and altered shape with increasing pCO_2 reported for other taxa in a novel taxon, *Amphiprion clarkii*. In addition, we report evidence of increasing otolith lateral development and surface roughness with increasing pCO_2. Impacts were observed in all otolith types, including the previously uninvestigated asterisci. We investigated each otolith type and side independently, observing asymmetrical responses to pCO_2 in lapilli and asterisci. Our experimental design and analysis facilitated construction of pCO_2 dose-response curves, which we created for all otolith types and sides in *A. clarkii* excepting right asterisci. These curves outline changes to multiple morphometric and mineralogical variables and may be leveraged to predict responses to pCO_2 conditions not investigated here. We speculate that these responses could impact auditory and/or vestibular sensitivity in teleosts, adding to previous observations and hypotheses involving sagittae and lapilli. In summary, our work adds to the existing knowledge base regarding otolith response to ocean acidification, which may aid in predicting and preserving teleost fitness in the near-future ocean.

ACKNOWLEDGMENTS

We would like to acknowledge Bill Robinson, Meng Zhou, Solange Brault, and Gene Gallagher for advice and guidance; Bryanna Broadaway, Alex Eisen-Cuadra, Ashley Bulseco-McKim, Jeremy Williams, Katie Flanders, and Nicole Henderson for assistance and support; and undergraduates from Roger Williams University who assisted with the experimental trial and data collection: Kristen Kiefer, Shawna Chamberlin, Jackie Mitchell, Drew Canfield, Allex Gourlay, and Matt Muscara.

633 **REFERENCES**

634

635 **Anken, R. H. and Rahmann, H.** (1999). Effect of altered gravity on the neurobiology of fish.
636 *Naturwissenschaften* **86**, 155–167.
637 **Anken, R. H., Ibsch, M. and Rahmann, H.** (1998). Neurobiology of fish under altered gravity
638 conditions. *Brain Res. Rev.* **28**, 9–18.
639 **Anken, R., Knie, M. and Hilbig, R.** (2017). Inner ear otolith asymmetry in late-larval cichlid
640 fish (*Oreochromis mossambicus*, Perciformes) showing kinetotic behaviour under
641 diminished gravity. *Sci. Rep.* **7**, 15630.
642 **Béarez, P., Carlier, G., Lorand, J. P. and Parodi, G. C.** (2005). Destructive and non-
643 destructive microanalysis of biocarbonates applied to anomalous otoliths of archaeological
644 and modern sciaenids (Teleostei) from Peru and Chile. *Comptes Rendus - Biol.* **328**, 243–
645 252.
646 **Beier, M.** (1999). On the influence of altered gravity on the growth of fish inner ear otoliths.
647 *Acta Astronaut.* **44**, 585–591.
648 **Bignami, S., Sponaugle, S. and Cowen, R. K.** (2013a). Response to ocean acidification in
649 larvae of a large tropical marine fish, *Rachycentron canadum*. *Glob. Chang. Biol.* **19**, 996–
650 1006.
651 **Bignami, S., Enochs, I. C., Manzello, D. P., Sponaugle, S. and Cowen, R. K.** (2013b). Ocean
652 acidification alters the otoliths of a pantropical fish species with implications for sensory
653 function. *Proc. Natl. Acad. Sci.* **110**, 7366–7370.
654 **Bignami, S., Sponaugle, S. and Cowen, R. K.** (2014). Effects of ocean acidification on the
655 larvae of a high-value pelagic fisheries species, Mahi-mahi *Coryphaena hippurus*. *Aquat.*
656 *Biol.* **21**, 249–260.
657 **Boulos, R. A., Zhang, F., Tjandra, E. S., Martin, A. D., Spagnoli, D. and Raston, C. L.**
658 (2015). Spinning up the polymorphs of calcium carbonate. *Sci. Rep.* **4**, 3616.
659 **Browning, Z. S., Wilkes, A. A., Moore, E. J., Lancon, T. W. and Clubb, F. J.** (2012). The
660 effect of otolith malformation on behavior and cortisol levels in juvenile red drum fish
661 (*Sciaenops ocellatus*). *Comp. Med.* **62**, 251–256.
662 **Byrne, R. H.** (1987). Standardization of standard buffers by visible spectrometry. *Anal. Chem.*
663 **59**, 1479–1481.

Caldeira, K. and Wickett, M. E. (2003). Oceanography: anthropogenic carbon and ocean pH. *Nature* **425**, 365–365.

Cattano, C., Calò, A., Di Franco, A., Firmamento, R., Quattrocchi, F., Sdiri, K., Guidetti, P. and Milazzo, M. (2017). Ocean acidification does not impair predator recognition but increases juvenile growth in a temperate wrasse off CO_2 seeps. *Mar. Environ. Res.* **132**, 33–40.

Checkley, D. M., Dickson, A. G., Takahashi, M., Radich, J. A., Eisenkolb, N. and Asch, R. (2009). Elevated CO_2 enhances otolith growth in young fish. *Science (80-.).* **324**, 1683–1683.

Chivers, D. P., Mccormick, M. I., Nilsson, G. E., Munday, P. L., Watson, S. A., Meekan, M. G., Mitchell, M. D., Corkill, K. C. and Ferrari, M. C. O. (2014). Impaired learning of predators and lower prey survival under elevated CO_2: a consequence of neurotransmitter interference. *Glob. Chang. Biol.* **20**, 515–522.

Coll-Lladó, C., Giebichenstein, J., Webb, P. B., Bridges, C. R. and De La Serrana, D. G. (2018). Ocean acidification promotes otolith growth and calcite deposition in gilthead sea bream (Sparus aurata) larvae. *Sci. Rep.* **8**, 1–10.

Doney, S. C., Fabry, V. J., Feely, R. A. and Kleypas, J. A. (2009). Ocean acidification: the other CO_2 problem. *Ann. Rev. Mar. Sci.* **1**, 169–192.

Esbaugh, A. J., Heuer, R. and Grosell, M. (2012). Impacts of ocean acidification on respiratory gas exchange and acid-base balance in a marine teleost, *Opsanus beta*. *J. Comp. Physiol. B Biochem. Syst. Environ. Physiol.* **182**, 921–934.

Fabry, V. J., Seibel, B. A., Feely, R. A., Fabry, J. C. O. and Fabry, V. J. (2008). Impacts of ocean acidification on marine fauna and ecosystem processes. *ICES J. Mar. Sci.* **65**, 414–432.

Faria, A. M., Filipe, S., Lopes, A. F., Oliveira, A. P., Gonçalves, E. J. and Ribeiro, L. (2017). Effects of high pCO_2 on early life development of pelagic spawning marine fish. *Mar. Freshw. Res.* **68**.

Fekete, D. M. (2003). Rocks that roll zebrafish. *Science* **302**, 241–2.

Nakamura Filho, A., Almeida, A. C. de, Riera, H. E., Araújo, J. L. F. de, Gouveia, V. J. P., Carvalho, M. D. de and Cardoso, A. V. (2014). Polymorphism of $CaCO_3$ and microstructure of the shell of a Brazilian invasive mollusc (*Limnoperna fortunei*). *Mater.*

Res. **17**, 15–22.

Franke, A. and Clemmesen, C. (2011). Effect of ocean acidification on early life stages of Atlantic herring (*Clupea harengus* L.). *Biogeosciences* **8**, 3697–3707.

Froese, R. and Pauly, D. (2018). Fishbase. *FishBase*.

Frommel, A. Y., Schubert, A., Piatkowski, U. and Clemmesen, C. (2013). Egg and early larval stages of Baltic cod, *Gadus morhua*, are robust to high levels of ocean acidification. *Mar. Biol.* **160**, 1825–1834.

Gagliano, M., Depczynski, M., Simpson, S. D. and Moore, J. A. (2008). Dispersal without errors: symmetrical ears tune into the right frequency for survival. *Proc. R. Soc. B Biol. Sci.* **275**, 527–534.

Gattuso, J. and Buddemeier, R. W. (2000). Calcification and CO_2. *Nature* **407**, 311–313.

Gaylord, B., Kroeker, K. J., Sunday, J. M., Anderson, K. M., Barry, J. P., Brown, N. E., Connell, S. D., Dupont, S., Fabricius, K. E., Hall-Spencer, J. M., et al. (2015). Ocean acidification through the lens of ecological theory. *Ecology* **96**, 3–15.

Grosell, M. (2011). Intestinal anion exchange in marine teleosts is involved in osmoregulation and contributes to the oceanic inorganic carbon cycle. *Acta Physiol. (Oxf).* **202**, 421–434.

Hamilton, T. J., Holcombe, A. and Tresguerres, M. (2013). CO_2-induced ocean acidification increases anxiety in Rockfish via alteration of $GABA_A$ receptor functioning. *Proc. R. Soc. B Biol. Sci.* **281**, 20132509–20132509.

Hendriks, I. E., Duarte, C. M. and Álvarez, M. (2010). Vulnerability of marine biodiversity to ocean acidification: a meta-analysis. *Estuar. Coast. Shelf Sci.* **86**, 157–164.

Heuer, R. M. and Grosell, M. (2014). Physiological impacts of elevated carbon dioxide and ocean acidification on fish. *AJP Regul. Integr. Comp. Physiol.* **307**, R1061–R1084.

Hilbig, R., Anken, R. H., Sonntag, G., Höhne, S., Henneberg, J., Kretschmer, N. and Rahmann, H. (2002). Effects of altered gravity on the swimming behaviour of fish. *Adv. Sp. Res.* **30**, 835–841.

Hurst, T. P., Fernandez, E. R., Mathis, J. T., Miller, J. A., Stinson, C. M. and Ahgeak, E. F. (2012). Resiliency of juvenile walleye pollock to projected levels of ocean acidification. *Aquat. Biol.* **17**, 247–259.

IPCC (2013). *Climate Change 2013: The Physical Science Basis. Contribution of Working Group I to the Fifth Assessment Report of the Intergovernmental Panel on Climate Change*.

(ed. Stocker, T. F.), Qin, D.), Plattner, G.-K.), Tignor, M.), Allen, S. K.), Boschung, J.), Nauels, A.), Xia, Y.), V., B.), and P.M., M.).

Ishimatsu, A., Kikkawa, T., Hayashi, M., Lee, K.-S. and Kita, J. (2004). Effects of CO_2 on marine fish: larvae and adults. *J. Oceanogr.* **60**, 731–741.

Ishimatsu, A., Hayashi, M. and Kikkawa, T. (2008). Fishes in high-CO_2, acidified oceans. *Mar. Ecol. Prog. Ser.* **373**, 295–302.

Jarrold, M. D. and Munday, P. L. (2018). Diel CO_2 cycles do not modify juvenile growth, survival and otolith development in two coral reef fish under ocean acidification. *Mar. Biol.* 165, 1–12.

Kikkawa, T., Ishimatsu, A. and Kita, J. (2003). Acute CO_2 tolerance during the early developmental stages of four marine teleosts. *Environ. Toxicol.* **18**, 375–382.

Kikkawa, T., Kita, J. and Ishimatsu, A. (2004). Comparison of the lethal effect of CO_2 and acidification on red sea bream (*Pagrus major*) during the early developmental stages. *Mar. Pollut. Bull.* **48**, 108–110.

Kroeker, K. J., Micheli, F. and Gambi, M. C. (2012). Ocean acidification causes ecosystem shifts via altered competitive interactions. *Nat. Clim. Chang.* **3**, 156–159.

Kroeker, K. J., Kordas, R. L., Crim, R., Hendriks, I. E., Ramajo, L., Singh, G. S., Duarte, C. M. and Gattuso, J. P. (2013). Impacts of ocean acidification on marine organisms: quantifying sensitivities and interaction with warming. *Glob. Chang. Biol.* **19**, 1884–1896.

Lai, F., Jutfelt, F. and Nilsson, G. E. (2015). Altered neurotransmitter function in CO_2-exposed stickleback (*Gasterosteus aculeatus*): a temperate model species for ocean acidification research. *Conserv. Physiol.* **3**, 1-6.

Le Quéré, C., Takahashi, T., Buitenhuis, E. T., Rödenbeck, C. and Sutherland, S. C. (2010). Impact of climate change and variability on the global oceanic sink of CO_2. *Global Biogeochem. Cycles* **24**, n/a-n/a.

Lychakov, D. V. and Rebane, Y. T. (2005). Fish otolith mass asymmetry: Morphometry and influence on acoustic functionality. *Hear. Res.* **201**, 55–69.

Ma, T., Kuroki, M., Miller, M. J., Ishida, R. and Tsukamoto, K. (2008). Morphology and microchemistry of abnormal otoliths in the ayu, *Plecoglossus altivelis*. *Environ. Biol. Fishes* **83**, 155–167.

Maneja, R. H., Frommel, A. Y., Geffen, A. J., Folkvord, A., Piatkowski, U., Chang, M. Y.

and Clemmesen, C. (2013). Effects of ocean acidification on the calcification of otoliths of larval Atlantic cod *Gadus morhua*. *Mar. Ecol. Prog. Ser.* **477**, 251–258.

Martino, J., Doubleday, Z. A., Woodcock, S. H. and Gillanders, B. M. (2017). Elevated carbon dioxide and temperature affects otolith development, but not chemistry, in a diadromous fish. *J. Exp. Mar. Bio. Ecol.* **495**, 57–64.

Martins, S. I. G. (2017). Impacts of CO_2-induced ocean acidification on predator detection ability and developementof temperate fish. *PhD thesis*, ISPA - Instituto Universitário de Ciências Psicológicas, Sociais e da Vida, Lisboa, Portugal.

Mikaloff Fletcher, S. E., Gruber, N., Jacobson, A. R., Doney, S. C., Dutkiewicz, S., Gerber, M., Follows, M., Joos, F., Lindsay, K., Menemenlis, D., et al. (2006). Inverse estimates of anthropogenic CO_2 uptake, transport, and storage by the ocean. *Global Biogeochem. Cycles* **20**, 1–16.

Millero, F. J., Zhang, J. Z., Fiol, S., Sotolongo, S., Roy, R. N., Lee, K. and Mane, S. (1993). The use of buffers to measure the pH of seawater. *Mar. Chem.* **44**, 143–152.

Mirasole, A., Gillanders, B. M., Reis-Santos, P., Grassa, F., Capasso, G., Scopelliti, G., Mazzola, A. and Vizzini, S. (2017). The influence of high pCO_2 on otolith shape, chemical and carbon isotope composition of six coastal fish species in a Mediterranean shallow CO_2 vent. *Mar. Biol.* **164**, 1–15.

Moyle, P. B. and Cech, J. J. (2004). *Fishes, An Introduction to Ichtyology*. 5th ed. (ed. Lee, C.), Chung, T.), Kuhl, M.), and Bradley, K.) San Francisco: Pearson Benjamin Cummings.

Mu, J., Jin, F., Wang, J., Zheng, N., Cong, Y. and Wang, J. Y. (2015). Effects of CO_2-driven ocean acidification on early life stages of marine medaka (*Oryzias melastigma*). *Biogeosciences* **12**, 3861–3868.

Munday, P. L., Jones, G. P., Pratchett, M. S. and Williams, A. J. (2008). Climate change and the future for coral reef fishes. *Fish Fish.* **9**, 261–285.

Munday, P. L., Crawley, N. E. and Nilsson, G. E. (2009). Interacting effects of elevated temperature and ocean acidification on the aerobic performance of coral reef fishes. *Mar. Ecol. Prog. Ser.* **388**, 235–242.

Munday, P. L., Gagliano, M., Donelson, J. M., Dixson, D. L. and Thorrold, S. R. (2011a). Ocean acidification does not affect the early life history development of a tropical marine fish. *Mar. Ecol. Prog. Ser.* **423**, 211–221.

788 **Munday, P. L., Hernaman, V., Dixson, D. L. and Thorrold, S. R.** (2011b). Effect of ocean
789 acidification on otolith development in larvae of a tropical marine fish. *Biogeosciences* **8**,
790 1631–1641.
791 **Munday, P. L., McCormick, M. I., Meekan, M. G., Dixson, D. L., Watson, S., Ferrari, M.**
792 **C. O. and Chivers, D. P.** (2012). Selective mortality associated with variation on CO_2
793 tolerance in a marine fish. *Ocean Acidif.* **1**, 1–5.
794 **Nilsson, G. E., Dixson, D. L., Domenici, P., McCormick, M. I., Sørensen, C., Watson, S.-A.**
795 **and Munday, P. L.** (2012). Near-future carbon dioxide levels alter fish behaviour by
796 interfering with neurotransmitter function. *Nat. Clim. Chang.* **2**, 201–204.
797 **Norman, G.** (2010). Likert scales, levels of measurement and the "laws" of statistics. *Adv. Heal.*
798 *Sci. Educ.* **15**, 625–632.
799 **Ohnishi, K., Yamamoto, T., Ogawa, Y., Takahashi, A., Yamashita, M. and Ohnishi, T.**
800 (2002). High transmittance of X-rays in the utricular otolith of upside-down swimming
801 catfish, *Synodontis nigriventris*. *Biol. Sci. Space.* **16**, 18–21.
802 **Orr, J. C., Fabry, V. J., Aumont, O., Bopp, L., Doney, S. C., Feely, R. A., Gnanadesikan,**
803 **A., Gruber, N., Ishida, A., Joos, F., et al.** (2005). Anthropogenic ocean acidification over
804 the twenty-first century and its impact on calcifying organisms. *Nature* **437**, 681–686.
805 **Oxman, D. S., Barnett-Johnson, R., Smith, M. E., Coffin, A., Miller, D. L., Josephson, R.**
806 **and Popper, A. N.** (2007). The effect of vaterite deposition on sound reception, ototlith
807 morphology, and inner ear sensory epithelia in hatchery-reared chinook salmon
808 (*Oncorhynchus tshawytscha*). *Can. J. Fish. Aquat. Sci.* **64**, 1469–1478.
809 **Panella, G.** (1971). Fish otoliths: daily growth layers and periodical patterns. *Science (80-.).*
810 **173**, 1124–1127.
811 **Perry, D. M., Redman, D. H., Widman, J. C., Meseck, S., King, A. and Pereira, J. J.** (2015).
812 Effect of ocean acidification on growth and otolith condition of juvenile scup, *Stenotomus*
813 *chrysops*. *Ecol. Evol.* **5**, 4187–4196.
814 **Pimentel, M. S., Faleiro, F., Dionisio, G., Repolho, T., Pousao-Ferreira, P., Machado, J. and**
815 **Rosa, R.** (2014). Defective skeletogenesis and oversized otoliths in fish early stages in a
816 changing ocean. *J. Exp. Biol.* **217**, 2062–2070.
817 **Popper, A. N. and Fay, R. R.** (1993). Sound detection and processing by fish: critical review
818 and major research questions. *Brain. Behav. Evol.*

Reimer, T., Dempster, T., Warren-Myers, F., Jensen, A. J. and Swearer, S. E. (2016). High prevalence of vaterite in sagittal otoliths causes hearing impairment in farmed fish. *Sci. Rep.* **6**, 25249.

Reimer, T., Dempster, T., Wargelius, A., Fjelldal, P. G., Hansen, T., Glover, K. A., Solberg, M. F. and Swearer, S. E. (2017). Rapid growth causes abnormal vaterite formation in farmed fish otoliths. *J. Exp. Biol.* **220**, 2965–2969.

Réveillac, E., Lacoue-Labarthe, T., Oberhänsli, F., Teyssié, J. L., Jeffree, R., Gattuso, J. P. and Martin, S. (2015). Ocean acidification reshapes the otolith-body allometry of growth in juvenile sea bream. *J. Exp. Mar. Bio. Ecol.* **463**, 87–94.

Ries, J. B., Cohen, A. L. and McCorkle, D. C. (2009). Marine calcifiers exhibit mixed responses to CO_2-induced ocean acidification. *Geology* **37**, 1131–1134.

Schade, F. M., Clemmesen, C. and Mathias Wegner, K. (2014). Within- and transgenerational effects of ocean acidification on life history of marine three-spined stickleback (*Gasterosteus aculeatus*). *Mar. Biol.* **161**, 1667–1676.

Seibel, B. A., Maas, A. E. and Dierssen, H. M. (2012). Energetic plasticity underlies a variable response to ocean acidification in the pteropod, *Limacina helicina antarctica*. *PLoS One* **7**, e30464.

Shen, S. G., Chen, F., Schoppik, D. E. and Checkley, D. M. (2016). Otolith size and the vestibulo-ocular reflex of larvae of white seabass *Atractoscion nobilis* at high pCO_2. *Mar. Ecol. Prog. Ser.* **553**, 173–182.

Simpson, S. D., Munday, P. L., Wittenrich, M. L., Manassa, R., Dixson, D. L., Gagliano, M. and Yan, H. Y. (2011). Ocean acidification erodes crucial auditory behaviour in a marine fish. *Biol. Lett.* **7**, 917–920.

Tomas, J. and Geffen, A. J. (2003). Morphometry and composition of aragonite and vaterite otoliths of deformed laboratory reared juvenile herring from two populations. *J. Fish Biol.* **63**, 1383–1401.

Victor, B. C. (1986). Delayed metamorphosis with reduced larval growth in a coral reef fish (*Thalassoma bifasciatum*). *Can. J. Fish. Aquat. Sci.* **43**, 1208–1213.

Wallace, R. B., Baumann, H., Grear, J. S., Aller, R. C. and Gobler, C. J. (2014). Coastal ocean acidification: The other eutrophication problem. *Estuar. Coast. Shelf Sci.* **148**, 1–13.

Wilcox-Freeburg, E. D. (2014). Exploring the link between otolith growth and function along

the biological continuum in the context of ocean acidification. *PhD thesis*, University of Massachusetts Boston, Boston, MA.

Wilcox-Freeburg, E., Rhyne, A., Robinson, W. E., Tlusty, M., Bourque, B. and Hannigan, R. E. (2013). A comparison of two pH-stat carbon dioxide dosing systems for ocean acidification experiments. *Limnol. Oceanogr. Methods* **11**, 485–494.

Table 1(on next page)

Summary of Observed Ocean Acidification Impacts on Otolith Morphology.

In the 'Metrics' column, S denotes effects of pCO_2 on sagittae and L denotes effects on lapilli. All metrics increased at elevated pCO_2 except where noted with *; these metrics decreased. The 'Min. Effect' column represents the minimum pCO_2 threshold for which any effect was observed, reported to the decimal place published. [1]Life stage, although unlisted in the manuscript, is here inferred from fish standard length (SL). [2]pCO_2 is unlisted in the manuscript and cannot be calculated without additional seawater carbonate chemistry parameter(s).

Citation	Species	Life Stage	Metrics	Min. Effect (µatm)
Checkley et al. 2009	*Atractoscion nobilis*	Larval	S Area	993
Munday et al. 2011b	*Amphiprion percula*	Larval	S Area, Length	1721.4
Hurst et al. 2012	*Theragra chalcogramma*	Juvenile	S Mean Incr. Width	478
Bignami et al. 2013a,b	*Rachycentron canadum*	Larval	S Mass; S,L Area, Vol., Dens., Area/Vol.*	800
Maneja et al. 2013	*Gadus morhua*	Larval	S,L Area; S Roundness; L Roundness*	1800
Bignami et al. 2014	*Coryphaena hippurus*	Larval	S,L Area	1190
Pimentel et al. 2014	*Solea senegalensis*	Larval	S Area	1600
Schade et al. 2014	*Gasterosteus aculeatus*	Juvenile	S Area	1167
Mu et al. 2015	*Oryzias melastigma*	Larval	S Area*	2372.6
Réveillac et al. 2015	*Sparus aurata*	Juvenile	S Calc. Rate, Area/TL, Roundness*	726
Shen et al. 2016	*Atractoscion nobilis*	Larval	S,L Area	2500
Faria et al. 2017	*Argyrosomus regius*	Larval	S Area, Perimeter, Width	1900
	Diplodus sargus	Larval	S Area, Perimeter	1100
	Solea senegalensis	Larval	S Area, Perimeter	1900
Martins 2017	*Lepadogaster lepadogaster*	Larval	S Roundness	1541.68
Mirasole et al. 2017	*Diplodus vulgaris*	Juvenile[1]	S Shape, Relative Length	pH 7.8[2]
	Gobius bucchichi	Adult[1]	S Shape	pH 7.8[2]
Coll-Lladó et al. 2018	*Sparus aurata*	Larval	S,L Area, Perimeter, Shape Irregularity	1159

1

Table 2(on next page)

Seawater carbonate chemistry parameters.

Values represent aquaria means (n = 3 for each treatment); standard deviations listed in parentheses for measured parameters.

Treatment (pH_T)	S (ppt)	T (°C)	A_T (µmol kg^{-1})	DIC (µmol kg^{-1})	pCO_2 (µatm)	Ω_{Ar}
8.16 (0.04)	35.00 (0.30)	28.20 (0.40)	2440 (147)	2018	299.4	4.84
7.80 (0.01)	35.00 (0.30)	28.20 (0.40)	2440 (152)	2237	825.5	2.54
7.60 (0.01)	35.00 (0.30)	28.30 (0.40)	2432 (140)	2318	1384.3	1.70
7.30 (0.01)	35.00 (0.30)	28.20 (0.40)	2418 (140)	2415	2897.0	0.89

1

Table 3(on next page)

Fish condition statistics.

Mortality and settlement values are means of all replicate aquaria percentages (n = 3 for each treatment); standard deviations listed in parentheses. Standard length values are combined means of all replicate aquaria means (n = 3 for each treatment); pooled standard deviations listed in parentheses.

pH Treatment	Mortality (%)	Settlement (%)	Standard Length (mm)
8.16	34 (24)	90 (6)	6.82 (0.26)
7.80	55 (4)	98 (3)	6.74 (0.29)
7.60	44 (8)	75 (9)	6.69 (0.25)
7.30	49 (34)	82 (5)	6.42 (0.19)

1

Table 4(on next page)

Otolith condition statistics.

Values are combined means of all replicate aquaria means (n = 3 for each treatment); pooled standard deviations listed in parentheses. Circularity is a dimensionless ratio. Lateral development is estimated on a scale of 1 (least developed) to 5 (most developed). Percent visible crystals is estimated on a scale of 5-50% visible crystals (i.e., surface area coverage).

Otolith	pH Treatment	Area (μm²)	Perimeter (μm)	Circularity	Lateral Development (1-5)	Percent Visible Crystals (5-50%)
LS	8.16	46480.70 (6229.33)	848.30 (67.26)	0.81 (0.06)	1.77 (0.75)	0.22 (0.12)
	7.80	48539.74 (6807.82)	865.16 (74.55)	0.82 (0.06)	3.21 (0.77)	0.40 (0.10)
	7.60	49544.93 (5234.76)	889.78 (64.66)	0.79 (0.07)	3.26 (1.07)	0.41 (0.11)
	7.30	48674.81 (6346.53)	878.97 (98.64)	0.80 (0.09)	3.60 (0.93)	0.41 (0.12)
RS	8.16	46100.48 (6190.66)	872.16 (299.17)	0.81 (0.10)	1.77 (0.72)	0.26 (0.10)
	7.80	49064.32 (6257.88)	869.39 (78.46)	0.82 (0.06)	3.01 (1.03)	0.37 (0.13)
	7.60	50075.38 (5095.22)	886.64 (67.06)	0.80 (0.07)	3.28 (0.92)	0.39 (0.10)
	7.30	49222.94 (6109.60)	875.83 (72.84)	0.81 (0.07)	3.78 (1.01)	0.43 (0.12)
LL	8.16	16375.95 (2703.31)	497.22 (48.74)	0.83 (0.07)	1.46 (0.56)	0.15 (0.07)
	7.80	17554.53 (2586.52)	510.53 (45.31)	0.85 (0.05)	1.37 (0.51)	0.14 (0.07)
	7.60	17559.28 (2226.09)	527.98 (51.63)	0.80 (0.09)	1.34 (0.51)	0.15 (0.06)
	7.30	17208.72 (2495.99)	510.27 (49.68)	0.83 (0.08)	1.68 (0.58)	0.20 (0.10)
RL	8.16	16016.49 (2645.01)	496.21 (51.38)	0.82 (0.08)	1.58 (0.50)	0.15 (0.09)
	7.80	17191.47 (2611.22)	511.93 (51.90)	0.83 (0.08)	1.33 (0.45)	0.14 (0.04)
	7.60	16916.55 (2575.21)	518.12 (57.31)	0.80 (0.09)	1.35 (0.51)	0.15 (0.05)
	7.30	17275.39 (2849.99)	508.70 (49.67)	0.84 (0.06)	1.72 (0.67)	0.19 (0.09)
LA	8.16	6547.43 (1356.95)	323.98 (54.10)	0.80 (0.09)	1.35 (0.52)	0.09 (0.03)
	7.80	6539.51 (1292.12)	318.68 (36.79)	0.80 (0.05)	1.32 (0.52)	0.09 (0.05)
	7.60	6540.09 (1079.92)	326.46 (29.16)	0.78 (0.11)	1.52 (0.37)	0.09 (0.02)
	7.30	6401.03 (993.74)	317.80 (26.22)	0.79 (0.08)	1.19 (0)	0.14 (0.02)
RA	8.16	5809.44 (1683.81)	302.05 (56.50)	0.79 (0.09)	1.41 (0.47)	0.10 (0.07)
	7.80	6550.19 (1443.81)	317.17 (43.24)	0.81 (0.06)	1.14 (0.33)	0.10 (0.05)
	7.60	6628.21 (1166.87)	328.70 (36.10)	0.78 (0.11)	1.27 (0.48)	0.08 (0.04)
	7.30	6234.35 (1126.96)	314.40 (33.66)	0.79 (0.08)	1.43 (0.79)	0.09 (0.04)

1

Table 5(on next page)

Component Variances and Loadings.

Loadings corresponding to various *Amphiprion clarkii* otolith morphological parameters, the variance of which composes the rotated components in Fig. 2 and other components that we excluded from the analysis. Also included are the variances associated with each component and the total variance associated with components.

Otolith	Component	Variance (%)	Area/SL	Perimeter/SL	Circularity	Lateral Development	Percent Visible Crystals
Left Sagittae	RC1	48	0.63	0.39	0.09	0.97	0.94
	RC2	37	0.62	0.84	-0.86	0.06	0.15
	Total	85					
Right Sagittae	RC1	57	0.74	0.68	0.01	0.95	0.97
	RC2	31	0.47	0.65	-0.94	0.09	-0.03
	Total	88					
Left Lapilli	RC1	45	-0.10	-0.32	0.70	0.88	0.94
	RC2	35	0.92	0.88	-0.22	-0.31	-0.06
	Total	80					
Right Lapilli	RC1	43	0.88	0.99	-0.64	-0.09	-0.02
	RC2	34	0.02	0.07	0.26	0.88	0.92
	Total	77					
Left Asterisci	RC1	44	0.80	0.82	-0.20	-0.76	-0.52
	RC2	34	-0.16	0.49	-0.92	0.00	0.75
	Total	78					
Right Asterisci	RC1	50	0.89	0.98	-0.73	-0.06	0.48
	RC2	24	-0.16	0.08	-0.31	0.91	0.50
	Total	74					

1

Figure 1

Effects of Seawater pCO_2 on Fish Condition.

(A) Odds of *Amphiprion clarkii* mortality by pH/pCO_2 treatment (legend). Regression lines (solid) and 95% confidence bands (dotted) represent significant relations between pH/pCO_2 treatment and (B) odds of on-time *A. clarkii* settlement ($p = 0.0279$); (C) *A. clarkii* standard length ($p = 0.0018$). Data points represent (A, B) binomial proportions by aquarium; (C) aquarium means. N = 12, n = 3 except where (B) 100% of fish in an aquarium settled on time (N = 10, n = 1 for pH 7.80 treatment only).

PeerJ Preprints | https://doi.org/10.7287/peerj.preprints.27040v1 | CC BY 4.0 Open Access | rec: 18 Jul 2018, publ: 18 Jul 2018

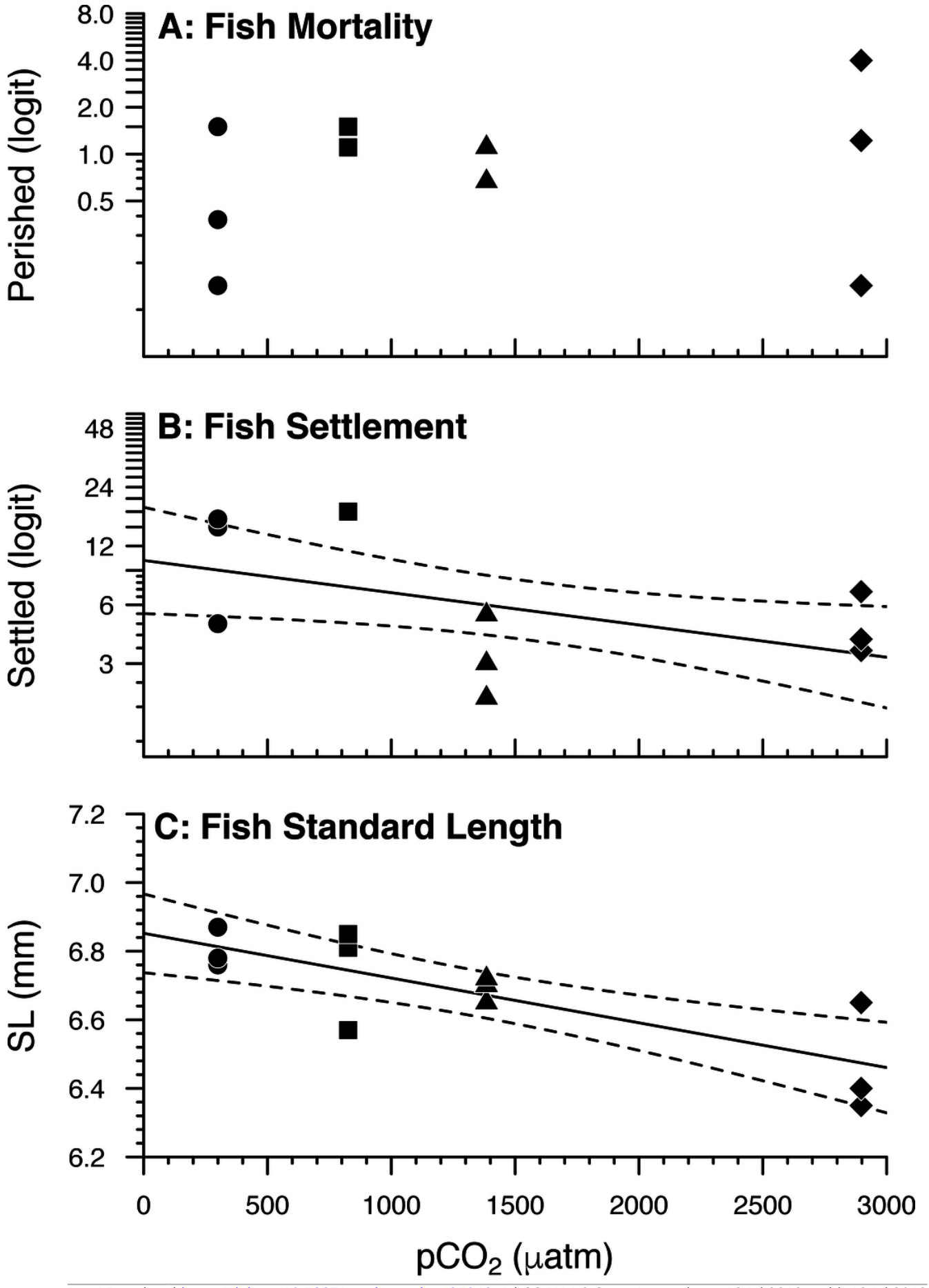

PeerJ Preprints | https://doi.org/10.7287/peerj.preprints.27040v1 | CC BY 4.0 Open Access | rec: 18 Jul 2018, publ: 18 Jul 2018

Figure 2

Effects of Seawater pCO_2 on Otolith Morphology.

Regression lines (solid) and 95% confidence bands (dotted) represent significant relations between pH/pCO_2 treatment (legend) and (A, B, C, D, E) rotated component (RC) scores representing *Amphiprion clarkii* otolith morphological variables, grouped by otolith type and side (A: p = 0.0061; B: p = 0.0004; C: p = 0.0045; D: p = 0.0168; E: p = 0.0420). Right asterisci components vs. pCO_2 did not yield significant relations, but RC2 scores are plotted for illustrative consistency. Data points represent aquaria. N = 12, n = 3 except where (E) no data is available for an aquarium (N = 11, n = 2 for pH = 7.30 treatment only). See Table 3 for otolith morphological variables and corresponding PCA loadings.

PeerJ Preprints | https://doi.org/10.7287/peerj.preprints.27040v1 | CC BY 4.0 Open Access | rec: 18 Jul 2018, publ: 18 Jul 2018